RSC Advances

This is an *Accepted Manuscript*, which has been through the Royal Society of Chemistry peer review process and has been accepted for publication.

Accepted Manuscripts are published online shortly after acceptance, before technical editing, formatting and proof reading. Using this free service, authors can make their results available to the community, in citable form, before we publish the edited article. This *Accepted Manuscript* will be replaced by the edited, formatted and paginated article as soon as this is available.

You can find more information about *Accepted Manuscripts* in the Information for Authors.

Please note that technical editing may introduce minor changes to the text and/or graphics, which may alter content. The journal's standard Terms & Conditions and the Ethical guidelines still apply. In no event shall the Royal Society of Chemistry be held responsible for any errors or omissions in this *Accepted Manuscript* or any consequences arising from the use of any information it contains.

ROYAL SOCIETY OF CHEMISTRY

www.rsc.org/advances

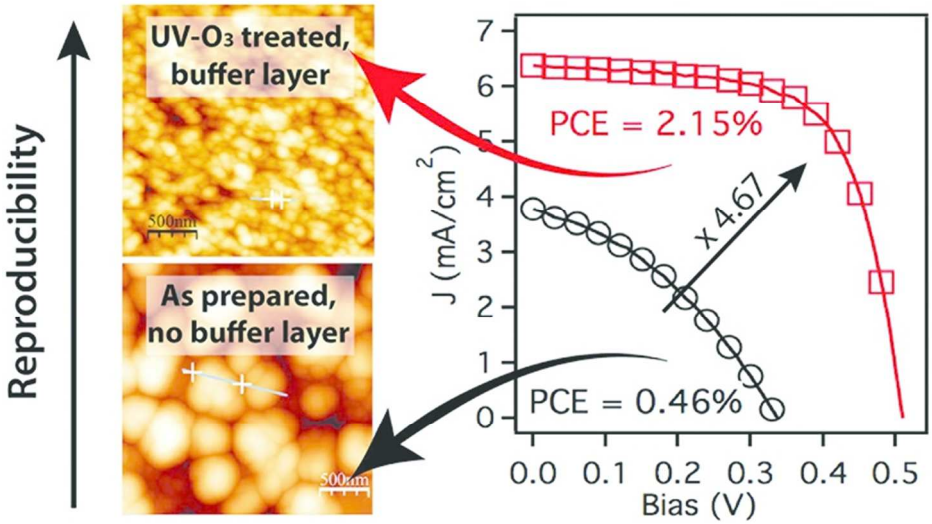

We report the processing conditions for fabricating efficient organic solar cells from aqueous dispersions of conjugated polymer nanoparticles.
74x40mm (300 x 300 DPI)

RSC Advances Accepted Manuscript

RSC Advances

RSCPublishing

PAPER

Fabrication Conditions for Efficient Organic Photovoltaic Cells from Aqueous Dispersions of Nanoparticles

Cite this: DOI: 10.1039/x0xx00000x

Monojit Bag,† Timothy S. Gehan,† Lawrence A. Renna, Dana D. Algaier, Paul M. Lahti and D. Venkataraman*

For environmentally friendly and cost-effective manufacturing of organic photovoltaic (OPV) cells, it is highly desirable to replace haloarenes with water as the active layer fabrication solvent. Replacing an organic solvent with water requires retooling the device fabrication steps. The optimization studies were conducted using poly(3-hexylthiophene) (P3HT) and [6,6]-phenyl C_{61} butyric acid methyl ester (PCBM) as active layer materials. These materials were dispersed in water as blend and separate nanoparticles using the miniemulsion method. Topologies of the active layers were investigated using atomic force microscopy and electron microscopy techniques. We have identified two essential steps to fabricate efficient OPVs from aqueous dispersions: (1) treatment of the hole-transport layer with UV-O_3 to make the surface hydrophilic and (2) the use of an electron-transporting buffer layer for efficient charge extraction. We have also identified relative humidity and substrate temperature as key fabrication parameters for obtaining uniform active layer films. The OPV devices were fabricated using PEDOT:PSS as the hole-transport layer and PCBM as electron-transport layer with Ca/Al as the counter electrode. Efficiencies of 2.15% with a fill factor over 66% were obtained; the efficiency and the fill-factor is the highest among all aqueous processing of P3HT:PCBM nanoparticle solar cells.

Received 00th January 2014,
Accepted 00th January 2014

DOI: 10.1039/x0xx00000x

www.rsc.org/

Broader context

OPV devices are lightweight, flexible, and portable, and they can be fabricated by techniques such as roll-to-roll processing over large areas at low cost. Thus, one can envision applications such as solar curtains, solar backpack chargers or solar chargers for powering personal devices. Driven by these possibilities, the past five years have witnessed an explosive growth in the area of organic photovoltaic cells. A key roadblock for large-scale manufacturing is the use of large amounts of halogenated arene solvents in the device fabrication. For cost-effective and energy-effective large-scale production of efficient OPVs that meets environmental and health safety standards, non-toxic solvents must be used for active layer fabrication. While OPVs have been fabricated from aqueous dispersions, the overall power conversion efficiency is still very low. By investigating and addressing the underlying scientific reasons for poor power conversion efficiency, we have developed protocol to fabricate reproducible and efficient OPVs.

1. Introduction

Active layers of organic photovoltaics (OPVs)[1] are typically fabricated using chloroarene solvents such as chlorobenzene. Large-scale fabrication[2] of OPVs using these solvents is challenging because chloroarenes have significant health and environmental hazards. The US Occupational Health and Safety Administration (OSHA) maximum allowed exposure limit for chlorobenzene is 75 ppm for an 8 h period.[3] In some EU countries, the maximum allowed exposure is 10 ppm because of possible nephrotoxicity and hepatotoxicity associated with chlorobenzene.[3,4] Although there have been some reports on using non-halogenated solvents for OPV fabrication,[5-7] the best device performance usually requires the use of chloroarene solvents. To enable cost-effective large-scale production of efficient OPVs that meets the environmental and health safety standards, it is imperative that fabrication methods are developed using non-toxic solvents.[8] Recently, there has been a widespread interest in using aqueous dispersions of conjugated polymer nanoparticles to fabricate active layers of OPVs.[9-14] However, low viscosity and de-wetting properties of polymer nanoparticle inks leads to non-uniform nanoparticle films, which makes device fabrication challenging. Therefore, the overall power conversion efficiency (PCE) of OPVs fabricated from aqueous dispersions has been very low.[9-11,13,14] Different strategies used by various groups to improve PCEs — such as

RSC Advances Accepted Manuscript

printing multiple layers of polymer ink,[14] and use of non-ionic fluorosurfactants (FSO-100)[9] — have met with limited success. Herein, we report a strategy to address effectively the major impediments for OPV active layer fabrication from aqueous dispersions: surface de-wetting leading to surface roughness and non-uniform films, and inefficient charge extraction. Commercially available regioregular poly(3-hexylthiophene) (P3HT, the electron donor) and [6,6]-phenyl C_{61} butyric acid methyl ester (PCBM, the electron acceptor) were used as active layer materials by an improved methodology for the fabrication of uniform and reproducible active layers from aqueous organic nanoparticle dispersions to give efficient charge extraction at the polymer/cathode interface.

2. Results and Discussion

2.1. Device optimization procedure: general approach

Conjugated polymer nanoparticles were synthesized using a modified mini-emulsion method.[15] Two types of nanoparticles were synthesized: blend nanoparticles containing both P3HT and PCBM in each nanoparticle,[16,17] and separate nanoparticles each only and separately containing P3HT or PCBM. Excess surfactant from as-prepared nanoparticle dispersions was removed by centrifugal filtration (see details in experimental section). We first prepared OPV devices using the protocol reported by Dastoor and co-workers,[18] but found that the nanoparticle aqueous dispersions did not wet the PEDOT:PSS substrates, resulting in patchy films. Our highest device PCE was much lower than the PCE reported for similar devices fabricated using this protocol. Interestingly, our PCEs were comparable those reported in another paper by the same authors using a similar procedure.[13] Also, over 90% of our devices failed with no PCE. The irreproducibility of the device fabrication indicated to us that reported protocol for fabrication of devices from aqueous dispersions was ineffective in our hands.

When a nanoparticle dispersion was coated onto PEDOT:PSS coated ITO substrates large aggregates of nanoparticles were observed in optical images (see in SI Fig. S1) as well as atomic force microscope (AFM) images (Fig. 1a). The presence of large aggregates (500 to 1000 nm range as shown in Fig. 1b) increases the surface r.m.s. roughness to ~70 nm. Upon deposition of the counter electrodes (Ca/Al), the devices show a large leakage current due to low shunt resistance (R_{sh}) which gives rise to low fill factor (*FF*) and open circuit voltage (V_{OC}). The typical R_{sh} value measured from a device was ~294 Ω-cm^2. We tried increased surfactant concentration to minimize aggregation, but found that excess surfactants can lead to dispersive charge transport, and did not consider it a viable solution.[19,20] We reasoned that the large aggregates of nanoparticles and crack formation in thin films are due to de-wetting of the polymer nanoparticle dispersion, consistent with the observations of Krebs and co-workers.[9] Therefore, to increase surface wettability, we exposed the PEDOT:PSS layer to UV-O_3 for few minutes. The contact angle of a water droplet on "as prepared" (without UV-O_3 treatment) PEDOT:PSS coated substrate was estimated to be advancing angle $\theta_A \approx 15°$ and receding angle $\theta_R \approx 8°$, whereas after UV-O_3 treatment, $\theta_A < 2°$ and water droplets spread very rapidly and uniformly. No large aggregates or cracks in the film were observed in optical images for devices using the UV-O_3 treatment. AFM of the nanoparticle films surface, as shown in Fig. 1c, shows that the surface r.m.s. roughness is ~14 nm. Although the R_{sh} of OPV devices prepared using this method increased significantly up to ~475 Ω-cm^2 after UV-O_3 treatment to the PEDOT:PSS layer, the series resistance (R_s) of these devices was still very high (on the order of 40 – 50 Ω-cm^2). Therefore, to increase charge extraction and reduce leakage current at the cathode/polymer interface, a thin PCBM buffer layer[21] was spin coated on top of the nanoparticle active layer. SEM image of the PCBM buffer layer is shown in Fig. 2.

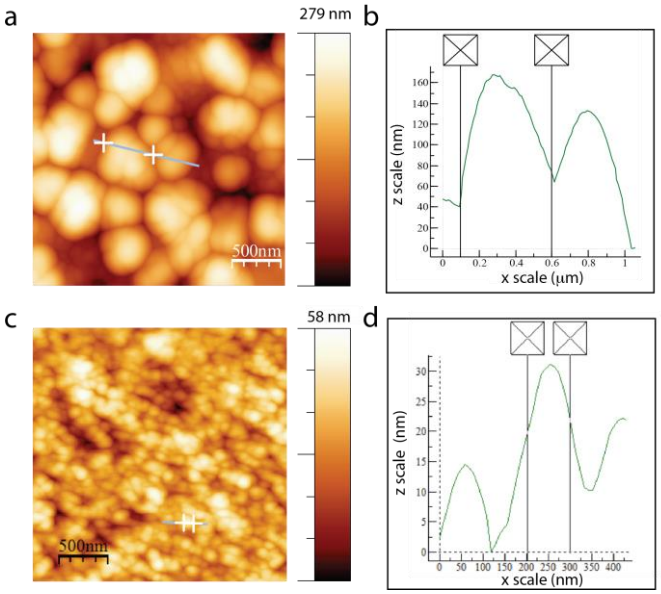

Fig. 1 (a) AFM image of P3HT:PCBM blend nanoparticles film spin coated on as prepared PEDOT:PSS coated ITO substrate. Average r.m.s. roughness is ~70 nm. (b) Line profile of the AFM image showing sub-micrometer to micrometer range of particle aggregates. (c) AFM image of P3HT:PCBM blend nanoparticles film spin coated on UV-O_3 treated PEDOT:PSS coated ITO substrate. Average r.m.s. roughness is ~14 nm. (c) Line profile of the AFM image showing nanoparticles of the order of 100 nm.

To probe the effect of the buffer layer on the charge transport through the nanoparticle assembly, conductive AFM (cAFM) measurements were performed. The cAFM in Fig. 3a shows areas of high 'hole' transport through a blend nanoparticle film with a PCBM buffer layer on top. The corresponding height image is shown in Fig. 3b with its corresponding line profile in Fig. 3c. These data indicate that the buffer layer reduces the 'hole' current at the cathode interface (the active layer surface) and also smoothens out the active layer's surface to an r.m.s. roughness of ~10 nm. When the buffer layer is removed by dipping the sample in dichloromethane (DCM) for a few seconds, efficient 'hole' transport through the remaining bulk of the film was observed, as seen in cAFM image in Fig. 3d and corresponding height

RSC Advances Accepted Manuscript

This journal is © The Royal Society of Chemistry 2014

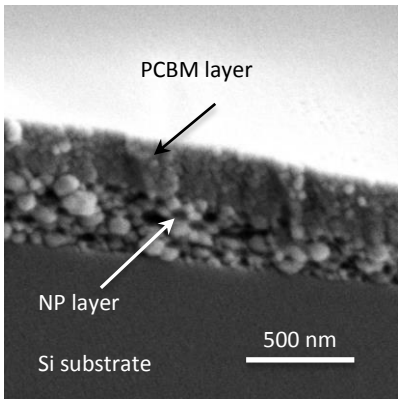

Fig. 2 Cross-sectional SEM image of P3HT:PCBM blend (1:1) nanoparticles spin coated on Si substrate. A thin layer of PCBM spin coated on top from 15 mg/mL solution in dichloromethane.

image shown in Fig. 3e. A comparison of the number of sites having particular cAFM hole transport ranges for pre-DCM wash versus post-DCM wash is shown in Fig. 3f. Nanoparticle OPVs retaining the PCBM buffer layer pre-wash showed much higher *FF* (up to 66%) and V_{OC} (up to 0.51 V) compared to the device without PCBM buffer layer (FF = 45% and V_{OC} = 0.43 V respectively). The R_s was decreased to ~10 Ω-cm^2 whereas R_{sh} was increased up to ~1.5 kΩ-cm^2. A further improvement in the V_{OC} was observed when nanoparticles films were washed with ethanol/water (1:1 by volume) mixture prior to deposition of the PCBM buffer layer: this removes excess surfactant from the surfaces and hence improves charge extraction.

To probe the effect of the nanoparticle assembly on the device performance, nanoparticle films were spin coated from ethanol/water mixed solvent. Significant improvement in the current density (J_{SC}) and PCE was observed when the polymer nanoparticles were re-suspended in 20 vol% ethanol in water before spin coating the nanoparticle dispersion. We believe the improvement in the current density is due to closer packing of the nanoparticles when spin coated from the 20 vol% ethanol solution by comparison to the packing of nanoparticles from water dispersion. The composition of the polymer ink plays a significant role to maximize nanoparticle close packing, which is driven by the interplay of interparticles forces (a) attractive hydrophobic force, mainly due to van der Waals interaction, and (b) repulsive electrostatic force due to ionic charge on the nanoparticles.[22]

Nanoparticle self-assembly can be tuned by varying the film drying-time, so two other external parameters—relative humidity (RH) and substrate temperature—needed to be optimized. The film drying process should not be so slow that first-coated PEDOT:PSS substrate layer gets dissolved by water from the next-coated nanoparticle dispersions. It is therefore important either to pre-heat the substrate or to heat the

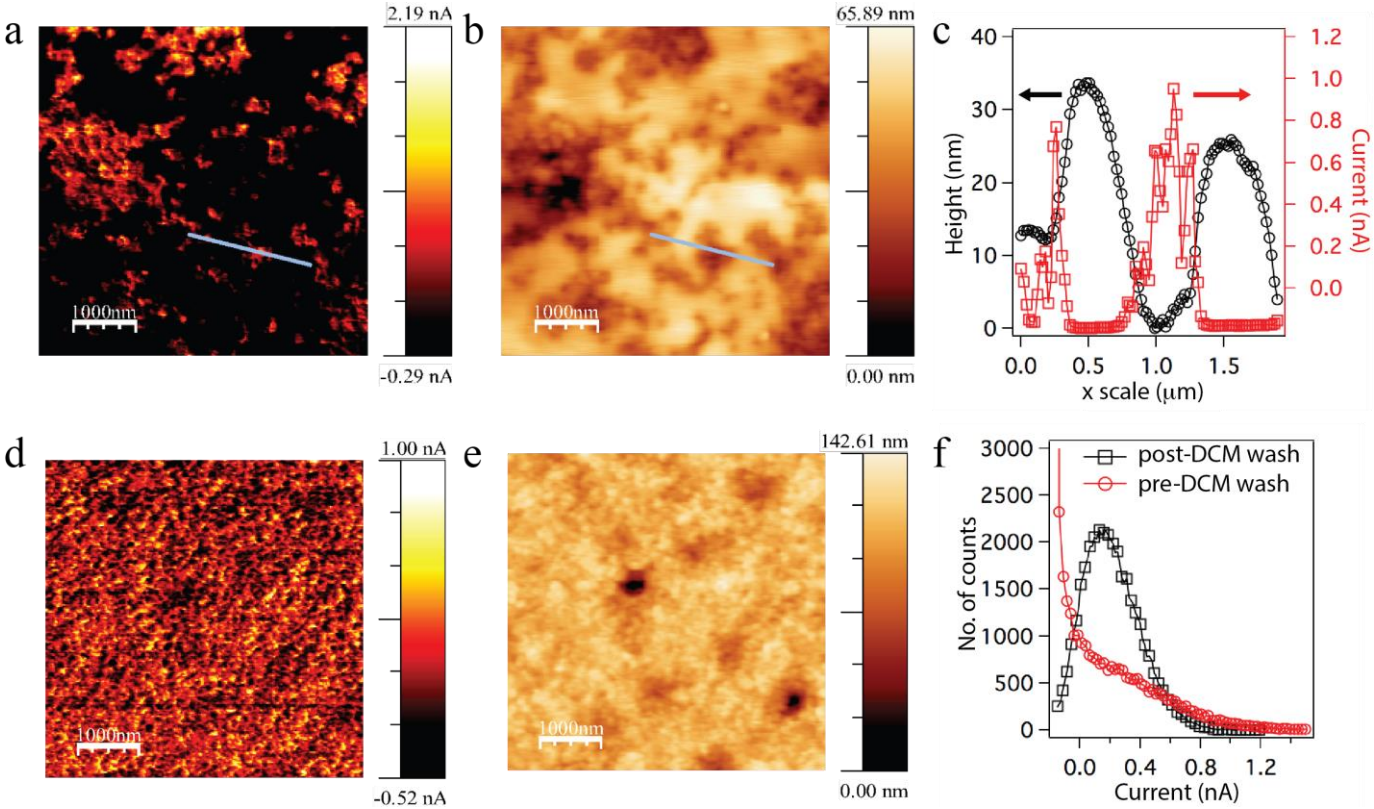

Fig. 3 (a) cAFM image of P3HT/PCBM blend nanoparticle device with PCBM buffer layer on top. (b) AFM topographic image of the same area. (c) Line profile of AFM height and current contrast image showing PCBM layer reduces leakage current. (d) cAFM image of the same film after washed with DCM. (e) AFM height image of the same area as mentioned in *d*. (f) Current distribution plot (number of pixels with particular current value measured by AFM probe tip under applied bias condition) of nanoparticles device with PCBM buffer layer (pre-DCM wash) as shown in *a* and after DCM wash (post-DCM wash) as shown in *b*.

RSC Advances Accepted Manuscript

substrates continuously while depositing the nanoparticle ink. We chose to heat the substrates radiatively using a commercial infrared (IR) lamp, because of its ability to heat the entire substrate more uniformly. The spin coater speed and amount of substrate pre-heating or heat treatment during spin coating then allows control of the film thickness. We found that >30% RH is necessary for uniform film formation. At low RH, films become porous and surface roughness increases. Also, at low RH (<23%) and during heating with the IR lamp, the formed film on the ITO substrate is rough and porous compared to film on the glass side, even though 40 nm of UV-O_3 treated PEDOT:PSS was present on both sides. Using an IR camera, we found that there is a difference in the absorption of the IR light between glass and ITO (see in SI Fig. S2). Therefore the IR lamp and relative humidity control both was necessary to derive jammed packed structure from thermodynamically and kinetically trapped assembly of nanoparticles.

Devices were fabricated using these improved processing conditions, and show a significant enhancement in PCE from 0.46% to 2.15%. As seen in Fig. 4 (see also in Table 1), the following necessary steps improve PCE from conditions used in processes **P1** to **P6**, as listed below.

Process **P1**: Nanoparticle active layer was spin coated onto "as prepared" PEDOT:PSS layer. Ca/Al electrode was thermally deposited on top.

Process **P2**: Active layer was spin coated on UV-O_3 treated PEDOT:PSS layer. Ca/Al electrode was thermally deposited on top.

Process **P3**: Active layer was spin coated onto "as prepared" PEDOT:PSS layer. A thin PCBM buffer layer was spin coated on top from a 15 mg/mL concentration in dichloromethane solution at 1000 rpm speed for 40 seconds, followed by Ca/Al electrode deposition.

Process **P4**: Active layer was spin coated onto UV-O_3 treated PEDOT:PSS substrate. A thin PCBM buffer layer was spin coated on top from a 15 mg/mL in dichloromethane concentration solution, followed by Ca/Al electrode deposition.

Process **P5**: Active layer was spin coated onto UV-O_3 treated

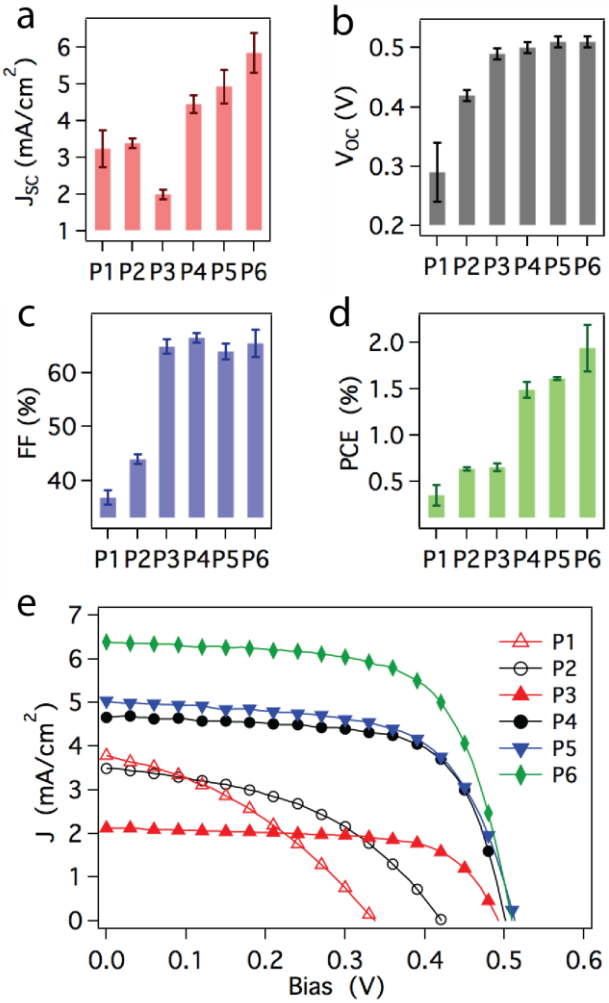

Fig. 4 (a-d) P3HT:PCBM blend nanoparticle device performance under different processing condition. (e) Current-voltage characteristic of the devices under AM 1.5G solar simulator at 100 mW/cm^2 light intensity.

Table 1: Performance of P3HT:PCBM blend nanoparticles devices fabricated from different processing conditions. Best-obtained values are given in parenthesis.

Processing conditions	J_{SC} (max) (mA/cm^2)	V_{OC} (max) (V)	*FF* (max) (%)	PCE (max) (%)	R_s (typical) (Ω cm^2)	R_{sh} (typical) (kΩ cm^2)
P1	3.25 (3.75)	0.29 (0.34)	36.8 (38.2)	0.35 (0.46)	47.5	0.29
P2	3.40 (3.52)	0.42 (0.43)	43.9 (44.8)	0.64 (0.66)	39.5	0.47
P3	2.0 (2.12)	0.49 (0.50)	64.8 (66.2)	0.65 (0.69)	24.0	2.50
P4	4.46 (4.69)	0.50 (0.51)	66.5 (67.4)	1.49 (1.58)	11.4	1.50
P5	4.94 (5.40)	0.51 (0.52)	64.0 (66.5)	1.61 (1.63)	13.8	1.51
P6	5.84 (6.38)	0.51 (0.52)	65.4 (67.9)	1.94 (2.15)	9.78	1.45

RSC Advances Accepted Manuscript

This journal is © The Royal Society of Chemistry 2014

PEDOT:PSS substrate. Active layer was then washed with 50% ethanol in water before PCBM buffer layer was spun on top followed by Ca/Al electrode deposition.

Process **P6**: 20% ethanol in water was added to nanoparticle dispersion before final centrifugal filtration. Active layer was then spin coated onto UV-O_3 treated PEDOT:PSS substrate. A thin PCBM buffer layer was then spin coated on top, followed by Ca/Al electrode deposition.

Except for the electrode evaporation step, the devices were fabricated in ambient atmosphere. We have also fabricated devices from separate P3HT and PCBM nanoparticles to prove the generality and reproducibility of the method with success rate over 80%.

2.2. Impact of post-heat treatment on device performance

Unlike in conventional solution film coating fabrication, in nanoparticle film coatings P3HT is in a semicrystalline aggregated structure prior to thin film formation. Therefore, one expects that thermal annealing should have minimal impact on the polymer crystallinity and hence the device PCE. In fact, in one literature example thermal annealing gave PCE decreases for P3HT:PCBM blend nanoparticle solar cells.[23] But, our results indicate that controlled heat treatment (post-heating) is required for optimum device performance using our fabrication protocol. Fig. 5a through 5d show device performances as a function of post fabrication heating temperature (see also in SI Fig. S3). In all the measurements, substrates were slowly heated from 30°C to the final temperature with a heating rate of 5 – 10°C/min. Significant improvement in the V_{OC} as well as the *FF* was observed when the devices were heated up to 80°C, which was well below the crystal re-orientation temperature (T_m ~ 195 °C) for P3HT reported in the literature.[24] We surmise that the slow heating of the substrate improves the interfacial interactions between polymer nanoparticles and the interlayer interactions between nanoparticles and electrodes.[25] The J_{SC} was increased only when devices were heated above 110°C. This could be due to PCBM cold crystallization which occurs in the temperature rage of 103 – 119°C for P3HT:PCBM blends of 1:1 by weight ratio.[24] P3HT crystallinity does not change upon heating to 150°C in x-ray diffraction measurements (see in SI Fig. S4), although a strong crystalline peak from PCBM grows after heating at 150°C. P3HT and PCBM are miscible and only one glass transition temperature (T_g) is observed at any binary composition between these; thus, any structural changes presumably happen during nanoparticle synthesis at a temperature 70°C, since T_g for the 1:1 P3HT:PCBM blend is less than 40°C.[26,27] However it should be noted that prolonged heating of these devices after fabrication results in a decrease of the efficiency.

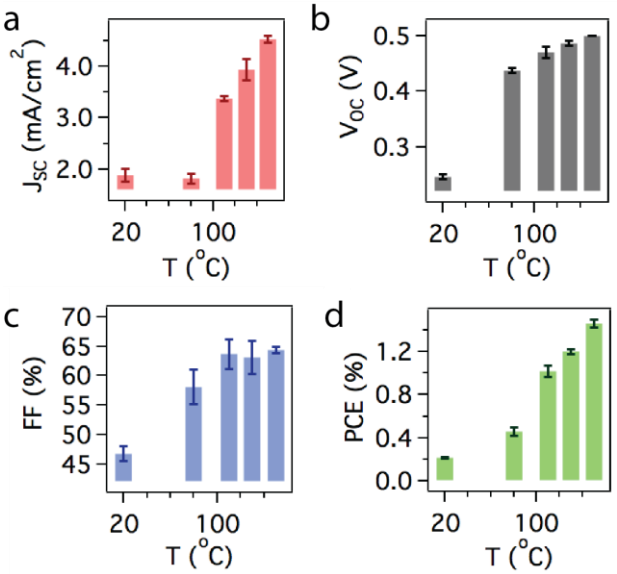

Fig. 5 P3HT:PCBM blend nanoparticles devices performance at different annealing temperature.

2.3. Light intensity dependent study, structure-properties correlation

To understand further the obtained device performance parameters, we carried out incident light intensity dependence measurements of I-V performance on a blend nanoparticle device with PCE ~2.0%. These are shown in Fig. 6a. The observed high *FF* over 67% even at 100 mW/cm^2 light intensity indicates a balanced transport of electron and holes to their respective electrodes and limited bimolecular recombination losses. A linear increase in J_{SC} with increasing light intensity was observed, as shown in the Fig. 6b. However, a slight drop in efficiency occurred as light intensity was decreased, mainly due to a drop in V_{OC}.

The cAFM measurements are a useful tool to probe the active layer morphology and how it is related to charge transport through the device active layer. As discussed above, the cAFM image in Figure 3a indicates that the PCBM buffer layer not only reduces the surface roughness (~10 nm), but also prevents leakage current by preventing undesired leakage hole transport to the top (cathode) electrode (Fig. 3c). Hence a significant improvement in *FF* and V_{OC} is observed in devices using this buffer, blocking layer. Upon washing devices with

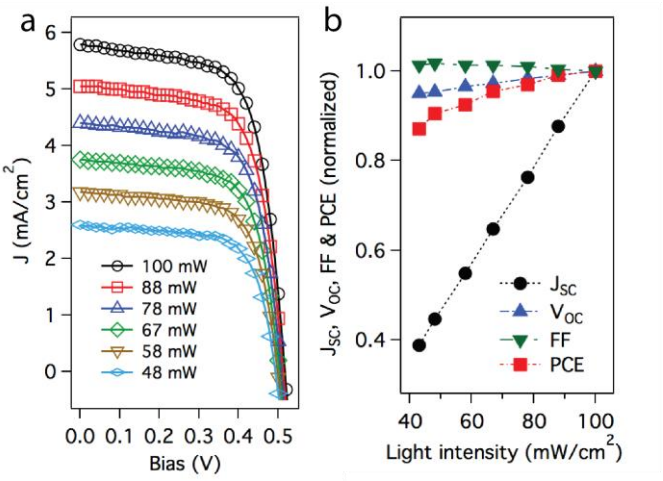

Fig. 6 (a) Light intensity dependent I-V curve of a P3HT:PCBM blend nanoparticle device. (b) Device parameters normalized with respect to 100 mW/cm^2 as a function of light intensity.

RSC Advances Accepted Manuscript

dichloromethane (DCM), this PCBM buffer layer was removed and the cAFM indicates that uniform conduction pathways remain for holes (Fig. 3d), which is in good agreement with the high J_{SC} observed in these devices. A quantitative analysis of conduction pathways with (Fig. 3a) and without (Fig. 3d) the PCBM buffer layer as shown in Fig. 3f is in good agreement with low leakage current and high FF observed in devices with a PCBM buffer layer. There is still some scope for improvements if we can reduce the non-uniformity in the PCBM buffer layer thickness as seen in Fig. 3b & 3c.

3. Conclusions

We have successfully fabricated efficient solar cells having up to 2.15% power conversion efficiencies using aqueous polymer nanoparticle dispersions by an environmentally low-impact procedure. One major challenge of reproducibly preparing uniform films from aqueous dispersions of nanoparticles was resolved by treatment of a PEDOT:PSS surface layer with UV-O_3 to increase surface wettability, and also by optimizing the nanoparticle ink formulation. We have also introduced use of a PCBM buffer layer between the nanoparticle active layer and the cathode electrode, which not only reduces the surface roughness, but also improves charge extraction at the cathode interface. Our future work will focus on processing electron transporting buffer layers from environmentally friendly solvents such as water or alcohols. Conducting AFM studies indicate there is a uniform distribution of conduction pathways throughout the nanoparticle active layer, consistent with the high current density observed in these devices. An observed *FF* > 66% was achieved, which is so far the highest reported for organic nanoparticle based OPV devices processed from aqueous dispersions. The morphology of the active layer, which is controlled by the hierarchical assembly of nano to mesoscale structures within and between the nanoparticles, presumably promotes the high *FF* in these devices. This constitutes a platform methodology for device fabrication, which could be easily applied to other active layer materials such as high performing low band-gap polymers or molecules to develop next generation devices with hierarchically controlled morphology. This methodology is also transferable to roll-to-roll processing, which would be very attractive for industrial processing of electronic devices.

4. Experimental

4.1 Materials and synthesis

Commercially available P3HT from Rieke Specialty Polymers with molecular weight 36 kDa, 96% regioregularity, and Đ = 2.3 was used without further purification. PCBM from NanoC was used as received. Dodecylsulfate sodium salt was used at 98% purity from Sigma Aldrich. Vivaspin 6 centrifugal filter tubes 10kDa MWCO PES membrane was obtained from Vivaproducts. A Misonix Sonicator 3000 ultrasonicator with a 1/8" probe tip from Qsonica was used to prepare the miniemulsions. A VWR Scientific Products Model 50T Aquasonic bath sonicator was used for initial solution preparation.

The nanoparticle dispersions were prepared using a modified miniemulsion method. The miniemulsion method requires the preparation of two solutions: a polymer in oil (chloroform) solution, and an aqueous surfactant solution. For blend nanoparticles both P3HT and PCBM were dissolved in chloroform, and for the separate nanoparticles either P3HT or PCBM was dissolved in chloroform. For blend nanoparticles, typically a 30 mg/mL (total) of P3HT and PCBM solution in chloroform and heated at 35˚C for at least 30 min with continuous stirring to ensure dissolution. A 10 mM SDS solution was prepared with nanopure water. To ensure dissolution of SDS, the solution was heated gently and sonicated. 3.0 mL of the 10 mM SDS solution was added to a 15 mL centrifuge tube. 0.3 mL of the 30 mg/mL blend chloroform solution was added to the surfactant solution. The outside of the centrifuge tube was immediately lowered into an ice bath and a 1/8" sonicator probe tip was lowered approximately half way into the solution and ultrasonicated at 20% max amplitude for 2 min. Immediately after sonicating, the emulsion solution was added to a glass vial and heated at 70˚C for 40 min with continuous stirring. The nanoparticle dispersion was then allowed to cool to room temperature. This solution was then repeated. Then both nanoparticle dispersions were added to a vivaspin 6 centrifugal filter tube. This centrifuge tube was centrifuged at 4180 relative centrifugal force (rcf) for 25 min. The filtrate was removed and the retentate was diluted to 5 mL with nanopure water. This process was repeated 3 more times. For the final (5^{th}) centrifugal filtration cycle, the retentate was diluted with 20 vol% ethanol in water and then centrifuged at 4180 rcf for 45 min. The retentate was then diluted to 0.5 mL with 20 vol% ethanol in water. This solution was then directly spin-coated onto the device substrates.

4.2 Device fabrication and characterization

Commercially available ITO substrates (TFD Inc, ~20 Ω/□) were cleaned by ultra-sonication in soap solution and distilled water, then by acetone, and by isopropyl alcohol. They were then kept in hot air oven at 140°C for 2 h. The substrates were then treated with UV-O_3 for 15 min (UVO cleaner, Jelight Company, Inc). Poly(3,4-ethylenedioxythiophene): Polystyrene sulfonate (PEDOT:PSS) (Clevios P VP AI 4083) was used as received and spin coated at 2500 rpm for 30 sec after filtering through 0.45 micron PVDF filter (Wilkem Scientific). PEDOT:PSS coated substrates were then annealed at 150°C for 20 minute in air, and allowed to cool to room temperature before again exposing to UV-O_3 for 3 min. Polymer nanoparticles of P3HT and PCBM were synthesized as described above and these solutions then used to spin coat active layers at 1000 r.p.m. for 60 seconds onto PEDOT:PSS-coated ITO substrates (either with or without UV-O_3 treatment of PEDOT:PSS layer, depending on the experimental). PEDOT:PSS layer without any UV-O_3 treatment may referre as "as prepared" PEDOT:PSS. A small humidifier was used to

RSC Advances Accepted Manuscript

 This journal is © The Royal Society of Chemistry 2014

control the humidity of the spin-coating deposition chamber, with the best power conversion results obtained for 30% chamber humidity. For some experiments, PEDOT:PSS coated substrates were pre-heated with the infrared lamp before or during nanoparticle active layer coating. As cast ITO/PEDOT:PSS/(nanoparticle) samples were then kept in a vacuum chamber for 10-12 h to remove excess water content in the films. For some samples, a thin layer of PCBM from 15 mg/mL in dichloromethane solution was spin coated atop the nanoparticle layer, at 1000 rpm for 40 s. Next, a 15 nm thick Ca electrode was thermally deposited at a rate of 0.5 Å/s, overlaid next by a 100 nm Al electrode deposited at a rate of 1 – 3 Å/s at a chamber pressure of 1×10^{-6} mbar. Devices were then annealed by slowly heating from room temperature to temperatures described earlier (inside a glove box under argon), then removed from the hot plate for performance measurements. AM1.5G solar simulator is used for device characterization with a light intensity of 100 mW/cm^2.

Acknowledgements

This work was supported as part of Polymer-Based Materials for Harvesting Solar Energy, an Energy Frontier Research Center funded by the U.S. Department of Energy, Office of Science, Basic Energy Sciences under Award #DE-SC0001087. We also thank the Amherst Fire Department for use of an infrared camera.

Notes and references

Department of Chemistry, University of Massachusetts, Amherst, USA
† These authors contributed equally
Email: dv@chem.umass.edu

Electronic Supplementary Information (ESI) available: [Optical microscopy image, infrared image, light IV curve and XRD data]. See DOI: 10.1039/c000000x/

Reference

1 W. Cao and J. Xue, *Energy Environ. Sci.*, 2014, **7**, 2123-2144.
2 T. R. Andersen, H. F. Dam, M. Hosel, M. Helgesen, J. E. Carle, T. T. Larsen-Olsen, S. A. Gevorgyan, J. W. Andreasen, J. Adams, N. Li, F. Machui, G. D. Spyropoulos, T. Ameri, N. Lemaitre, M. Legros, A. Scheel, D. Gaiser, K. Kreul, S. Berny, O. R. Lozman, S. Nordman, M. Valimaki, M. Vilkman, R. R. Sondergaard, M. Jorgensen, C. J. Brabec and F. C. Krebs, *Energy Environ. Sci.*, 2014, DOI: 10.1039/C1034EE01223B.
3 In *Limits for Air Contaminants In "Toxic and Hazardous Substances (1910.1000 Table Z-1) (Standards -29 CFR)*; Administration, O. S. H., Ed.; United States Dept. of Labor, 2005.
4 U. Knecht and H. J. Woitowitz, *Int. Arch. Occup. Environ. Health*, 2000, **73**, 543-554.
5 C.-C. Chueh, K. Yao, H.-L. Yip, C.-Y. Chang, Y.-X. Xu, K.-S. Chen, C.-Z. Li, P. Liu, F. Huang, Y. Chen, W.-C. Chen and A. K. Y. Jen, *Energy Environ. Sci.*, 2013, **6**, 3241-3248.
6 X. Guo, M. Zhang, C. Cui, J. Hou and Y. Li, *ACS Appl. Mater. & Interfaces*, 2014, **6**, 8190-8198.
7 B. Schmidt-Hansberg, M. Sanyal, N. Grossiord, Y. Galagan, M. Baunach, M. F. G. Klein, A. Colsmann, P. Scharfer, U. Lemmer, H. Dosch, J. Michels, E. Barrena and W. Schabel, *Sol. Energy Mater. Sol. Cells*, 2012, **96**, 195-201.
8 R. Søndergaard, M. Helgesen, M. Jørgensen and F. C. Krebs, *Adv. Energy Mater.*, 2011, **1**, 68-71.
9 T. R. Andersen, T. T. Larsen-Olsen, B. Andreasen, A. P. L. Böttiger, J. E. Carlé, M. Helgesen, E. Bundgaard, K. Norrman, J. W. Andreasen, M. Jørgensen and F. C. Krebs, *ACS Nano*, 2011, **5**, 4188-4196.
10 T. Kietzke, D. Neher, M. Kumke, R. Montenegro, K. Landfester and U. Scherf, *Macromolecules*, 2004, **37**, 4882-4890.
11 T. Kietzke, D. Neher, K. Landfester, R. Montenegro, R. Guntner and U. Scherf, *Nat. Mater.*, 2003, **2**, 408-U407.
12 J. A. Labastide, M. Baghgar, I. Dujovne, Y. P. Yang, A. D. Dinsmore, B. G. Sumpter, D. Venkataraman and M. D. Barnes, *J. Phys. Chem. Lett.*, 2011, **2**, 3085-3091.
13 N. Nicolaidis, B. Vaughan, C. J. Mulligan, G. Bryant, T. Zillger, B. Trnovec, A. C. Hübler, N. Holmes, N. A. Cooling, M. J. Griffith, C. Bilen, P. Kumar, K. Feron, X. Zhou, D. Elkington, W. J. Belcher and P. C. Dastoor, *Appl. Phys. Lett.*, 2014, **104**, 043902.
14 A. Stapleton, B. Vaughan, B. Xue, E. Sesa, K. Burke, X. Zhou, G. Bryant, O. Werzer, A. Nelson, A. L. David Kilcoyne, L. Thomsen, E. Wanless, W. Belcher and P. Dastoor, *Sol. Energy Mater. Sol. Cells*, 2012, **102**, 114-124.
15 K. Landfester In *Colloid Chemistry II*, 2003; Vol. 227.
16 S. Chambon, C. Schatz, V. Sebire, B. Pavageau, G. Wantz and L. Hirsch, *Mater. Horiz.*, 2014, **1**, 431-438.
17 J. J. Richards, C. L. Whittle, G. Shao and L. D. Pozzo, *ACS Nano*, 2014, **8**, 4313-4324.
18 S. Ulum, N. Holmes, D. Darwis, K. Burke, A. L. David Kilcoyne, X. Zhou, W. Belcher and P. Dastoor, *Sol. Energy Mater. Sol. Cells*, 2013, **110**, 43-48.
19 M. Bag, T. S. Gehan, D. D. Algaier, F. Liu, G. Nagarjuna, P. M. Lahti, T. P. Russell and D. Venkataraman, *Adv. Mater.*, 2013, **25**, 6411-6415.
20 X. Han, M. Bag, T. S. Gehan, D. Venkataraman and D. Maroudas, *Chem. Phys. Lett.*, 2014, **610-611**, 273-277.
21 S. Cho, K.-D. Kim, J. Heo, J. Y. Lee, G. Cha, B. Y. Seo, Y. D. Kim, Y. S. Kim, S.-y. Choi and D. C. Lim, *Sci. Rep.*, 2014, **4**.
22 R. M. Choueiri, A. Klinkova, H. Thérien-Aubin, M. Rubinstein and E. Kumacheva, *J. Am. Chem. Soc.*, 2013, **135**, 10262-10265.
23 D. Darwis, N. Holmes, D. Elkington, A. L. David Kilcoyne, G. Bryant, X. Zhou, P. Dastoor and W. Belcher, *Sol. Energy Mater. Sol. Cells*, 2014, **121**, 99-107.
24 E. Verploegen, R. Mondal, C. J. Bettinger, S. Sok, M. F. Toney and Z. Bao, *Adv. Funct. Mater.*, 2010, **20**, 3519-3529.
25 D. Chen, A. Nakahara, D. Wei, D. Nordlund and T. P. Russell, *Nano Lett.*, 2010, **11**, 561-567.
26 J. Zhao, A. Swinnen, G. Van Assche, J. Manca, D. Vanderzande and B. V. Mele, *J. Phys. Chem. B*, 2009, **113**, 1587-1591.
27 N. Trinh Tung, N. Duc Nghia and N. Van Tuyen, *Adv. Nat. Sci: Nanosci. Nanotechnol.*, 2012, **3**, 045001.

RSC Advances Accepted Manuscript